Environ. Sci. Technol. **2005**, *39,* 6420−6428

Inhibition of Calcite Precipitation by Natural Organic Material: Kinetics, Mechanism, and Thermodynamics†

YI-PIN LIN,‡ PHILIP C. SINGER,*,‡ AND GEORGE R. AIKEN§

Department of Environmental Sciences and Engineering, University of North Carolina, CB #7431, Chapel Hill, North Carolina 27599-7431, and U.S. Geological Survey, 3215 Marine Street, Boulder, Colorado 80303

The inhibition of calcite precipitation by natural organic material (NOM) in solutions seeded with calcite was investigated using a pH-stat system. Experiments were carried out using three NOMs with different physical/chemical properties. For each of the materials, inhibition was found to be more effective at lower carbonate/calcium ratios and lower pH values. The reduction in the precipitation rate could be explained by a Langmuir adsorption model using a conditional equilibrium constant. By identification of the type of site on the NOM molecules that is involved in the adsorption reaction, the "conditional" equilibrium constants obtained at different solution compositions converged to a single "nonconditional" value. The thermodynamic data determined at 25 °C and 1 atm suggest that the interaction between NOM molecules and the calcite surface is chemisorptive in nature and that adsorption is an endothermic reaction driven by the entropy change. The greatest degree of inhibition was observed for the NOM with the highest molecular weight and aromatic carbon content. For a given type of NOM, the degree of inhibition of calcite precipitation was dictated by the balance between the enthalpy change and the entropy change of the adsorption reaction.

Introduction

Calcite is one of the most reactive minerals at the earth's surface. Both crystallization and dissolution of calcite play important roles in aquatic chemistry and geochemistry because calcite, coupled with atmospheric carbon dioxide, regulates the buffering capacity of the aquatic system and influences aqueous phase reactions involving calcium and carbonates (*1*). It is well-known, however, that natural organic matter (NOM) interacts strongly with calcium carbonate and acts as an inhibitor to calcium carbonate crystal growth in aquatic systems (*2*−*5*). While it has been observed that differences in NOM composition influence calcite behavior in aquatic environments to varying degrees (*3*, *5*), the underlying chemistry driving these interactions remains poorly defined.

Adsorption of organic ligands onto a mineral surface can either promote the dissolution of the mineral in undersaturated solutions (*6*) or inhibit the precipitation of the mineral in supersaturated solutions. In aquatic environments that are supersaturated with respect to calcite, the precipitation of calcite is thermodynamically favored. Supersaturation with respect to calcite, however, is commonly observed in waters rich in NOM (*3*). It is suggested that NOM acts as an inhibitor to calcium carbonate precipitation by blocking the active growth sites through adsorption reactions (*4*, *5*, *7*). Although the "blockage" theory is widely accepted, the manner by which NOM is adsorbed on the calcite surface is not well understood. At the present time, the kinetics of calcite precipitation in the presence of NOM can only be described by empirical rate expressions (*4*, *8*−*10*).

The physical and chemical properties of NOM that have been proposed to relate to inhibition include hydrophobicity, functionality, and molecular size (*5*). Zulling and Morse (*11*) reported that fatty acids have an increasing affinity for a calcite surface with increasing alkyl chain length, which can be explained by the hydrophobic effect (*1*). The hydrophobic nature of the inhibitor may also lead to an entropy-driven adsorption process that causes more complete surface coverage and, consequently, greater inhibition of mineral precipitation (*12*). The carboxyl fraction contributes to the hydrophilicity of NOM. At neutral pH, these carboxyl groups exist in their deprotonated forms and have a great affinity for free aqueous calcium ions. However, previous studies show that the complexation of Ca^{2+} with the carboxyl moieties of NOM in the solution phase, thereby changing the degree of supersaturation with respect to calcite, is not an important consideration for altering calcite precipitation kinetics (*4*, *5*). Inskeep and Bloom (*4*) documented that aromaticity is the property that causes the strongest growth inhibition. They demonstrated that the aromatic polymeric constituents from a soil fulvic acid are more effective than nonpolymeric or less aromatic organic compounds in a soil−water extract in inhibiting calcite precipitation. Another important property related to the inhibition of calcite precipitation is molecular size. Organic acids with higher molecular weights were found to be more effective in the inhibition of calcite precipitation than those with lower molecular weights. The stereochemical effect, e.g., high molecular weight molecules facilitate the blockage of the crystal growth sites on the mineral surface, was suggested as the major reason (*7*). Grossl and Inskeep (*12*) investigated the inhibition of octacalcium phosphate in the presence of humic, fulvic, and tannic acids. They concluded that the most effective inhibitor was humic acid, followed by fulvic acid and tannic acid, which coincided with the order of molecular size and hydrophobicity. Although it has been demonstrated that NOM characteristics can affect its inhibitory ability, the relationship between these characteristics and the thermodynamics of the responsible reaction is still undefined.

Calcite precipitation involves heterogeneous reactions, such as adsorption of lattice ions and incorporation of adsorbed ions into the mineral lattice. With the help of a calcite surface complexation model (*13*, *14*), calcite precipitation kinetics can be described in terms of calcite surface speciation (*15*, *16*). In this paper, we expand on the understanding of the mechanisms driving calcite precipitation by describing the results of experiments designed to determine the influence of NOM on these mechanisms. Specifically, the objectives of this research are to (1) investigate the kinetics of calcite precipitation in the presence of NOM with different characteristics, (2) determine the mechanism(s) responsible for the inhibition of calcite precipitation by NOM on the molecular scale, (3) provide

† This paper is part of the Charles O'Melia tribute issue.

* Corresponding author phone: (919)966-3865; fax: (919)966-7911; e-mail: phil_singer@unc.edu.

‡ University of North Carolina.

§ U.S. Geological Survey.

10.1021/es050470z CCC: $30.25
Published on Web 07/27/2005

thermodynamic information for the inhibitory reaction(s), and (4) determine the important physical/chemical properties of NOM that are responsible for the inhibition of calcite precipitation. Better understanding of the processes occurring at the calcite−water interface will improve our knowledge of how NOM is adsorbed on the calcite surface and how the adsorbed NOM affects calcite precipitation.

Material and Methods

pH-stat System. To study the effects of NOM on calcite precipitation kinetics, a pH-stat system was utilized (*5*, *16*, *17*). The system maintains a constant degree of supersaturation with respect to calcite during the course of the experiment. A schematic of the system is shown in Figure S1 of the Supporting Information, along with a detailed description of the system and the principles underlying the experimental design.

For each experiment, the pH value was set at a target value to achieve and maintain the desired degree of supersaturation. The pH-stat system ensured that the precipitation experiment was performed at the target pH value ± 0.05 pH units. The degree of supersaturation (Ω) is defined as follows

$$\Omega = \frac{(Ca^{2+})(CO_3^{2-})}{K_{sp}} \quad (1)$$

where (Ca^{2+}) and (CO_3^{2-}) are the activities of calcium and carbonate ions in the solution, respectively, and K_{sp} ($10^{-8.48}$ at 25 °C) is the solubility product of calcite. The volume of $CaCl_2$ and Na_2CO_3 added to compensate for calcite precipitation is monitored continuously over time.

Working Solutions and Chemicals. To prevent homogeneous calcite precipitation, 1 L of a working solution with Ω = 5.3 was freshly prepared from equal volumes of $CaCl_2$ and $NaHCO_3$ solutions before each experiment. $CaCl_2$ and $NaHCO_3$ solutions were prepared using reagent-grade chemicals (Fisher Chemical Co.) and deionized water. Solutions with four different C_T/Ca^{2+} molar ratios ranging from 0.5 to 10 (C_T is the total inorganic carbon concentration), pH values ranging from 7.68 to 9.01, and temperatures in the range of 15−45 °C were tested, as shown in Table S1 of the Supporting Information. The ionic strength of the working solution was adjusted to 0.1 with KCl. Solutions of 0.1 M NaOH or HCl were used to adjust the pH to achieve the desired Ω value. For each solution, 0−5 mg/L of NOM was added to investigate its inhibitory effects. No homogeneous precipitation occurred over a time course of more than 4 h at this degree of supersaturation as shown by a constant pH value observed during this period.

Crystallization Experiments. Appoximately 150 mg of reagent-grade calcite particles (Fisher Scientific) were added to 500 mL of the working solution to initiate calcite precipitation. The calcite particles had a specific surface area of 0.278 m^2/g as determined by the three-point N_2−Brunauer−Emmett−Teller (BET) method (*18*). The solution was mixed by a magnetic stirring bar at 600 rpm. All experiments were conducted for 90 min under 1 atm with ambient levels of CO_2. After the addition of calcite particles, the solution pH started to decrease as a result of calcite precipitation. Given the lack of observed precipitation in the solution in the absence of calcite particles, all crystal growth is expected to have occurred on the calcite particle surfaces after the calcite was introduced. Titrant ($CaCl_2$ and Na_2CO_3) addition and pH were continuously recorded as functions of time. Typical titrant addition data for the crystallization experiments in the presence of NOM are shown in Figure S2 in the Supporting Information. The initial slope of the titrant addition versus time curve was used to estimate the initial rate of calcite precipitation. The calcite precipitation rate was found to be proportional to the available surface area of the seed in preliminary experiments (*16*). The kinetic data reported in this study were normalized by the surface area.

The seed materials were collected and dried at 35 °C overnight after the completion of several precipitation experiments. X-ray diffraction (XRD) analysis (Rigaku MultiFlex, Rigaku/MSC) was performed on the dried material. XRD results indicated that calcite was the only phase precipitated.

Natural Organic Materials. Suwannee River fulvic acid (SRFA; IHSS Reference FA), Pacific Ocean fulvic acid (POFA), and Williams Lake hydrophobic organic acid (WLHPOA) were chosen to investigate the inhibition of calcite precipitation due to their distinctly different physical/chemical characteristics. These materials were isolated on Amberlite XAD-8 resin according to the methods described by Aiken et al. (*19*). Quantitative ^{13}C NMR spectra were measured on solutions of approximately 100 mg/mL of the sodium salt of each isolate dissolved in H_2O-D_2O (1:1), adjusted to pH 7, in 10 mm tubes on a Varian spectrometer (Model 300) at 75.429 MHz using inverse gated decoupling with an 8 s delay (*20*). The ^{13}C NMR spectra were electronically integrated (*21*). The region from 110 to 160 ppm was assigned as the aromatic region of the spectrum (*22*); the aromatic carbon content of the three samples ranged from 7.3% to 28%. Elemental composition of the isolates was determined at Huffman Laboratories (Golden, CO) by methods discussed by Huffman and Stuber (*23*); the carbon content of the three samples ranged from 52.7% to 56.2%. Specific ultraviolet absorbance (SUVA) data were determined on solutions containing approximately 5 mg C/L of isolated material in distilled water with values ranging from 0.6 to 3.6 L/(mg m). Weight-average molecular weights (M_w) were determined using high-pressure size exclusion chromatography (HPSEC) (*24*), with values ranging from 532 to 1360 g/mol. Detailed chemical characteristics of the three NOM samples are presented in Table S2 of the Supporting Information.

Titration of NOM. A 50 mL stock solution with 300 mg/L of NOM was prepared. The ionic strength of the stock solution was adjusted to 0.1 with 4 M KCl solution. An Accumet pH meter coupled with a calomel combination pH electrode previously calibrated with pH 4.00, 7.00, and 10.00 standard buffers was used to monitor pH. The NOM stock solution was purged with nitrogen for 30 min and then continuously stirred under a nitrogen atmosphere to avoid interference by carbon dioxide acidity. The initial pH of the solution was recorded. A 10 mL buret filled with 0.04 M NaOH was used for titration. Approximately 0.1 mL of the NaOH titrant was added stepwise, and 60 s was allowed for pH equilibration. The added volume of the titrant and the pH were recorded after each titrant addition. The charge density of NOM, based on a charge balance of the solution, is given by eq 2

$$\text{charge density (equiv/g NOM)} = \frac{[A^-]}{V_0 C} = \frac{[H^+] + [Na^+] - [OH^-]}{V_0 C} \quad (2)$$

where $[A^-]$ is the net charge of NOM in equivalents per liter, V_0 is the initial sample volume, and C is the concentration of NOM of the sample (g as NOM/L).

Calculation of Solution and Calcite Surface Speciation. Visual MINTEQ, version 2.30 (*25*), was used for calculation of solution speciation and calcite surface speciation under our experimental conditions. The thermodynamic data for solution-phase reactions in the database of Visual MINTEQ, version 2.30, were employed without modification. The calculation of calcite surface speciation was based on the surface complexation model proposed by van Cappellen et

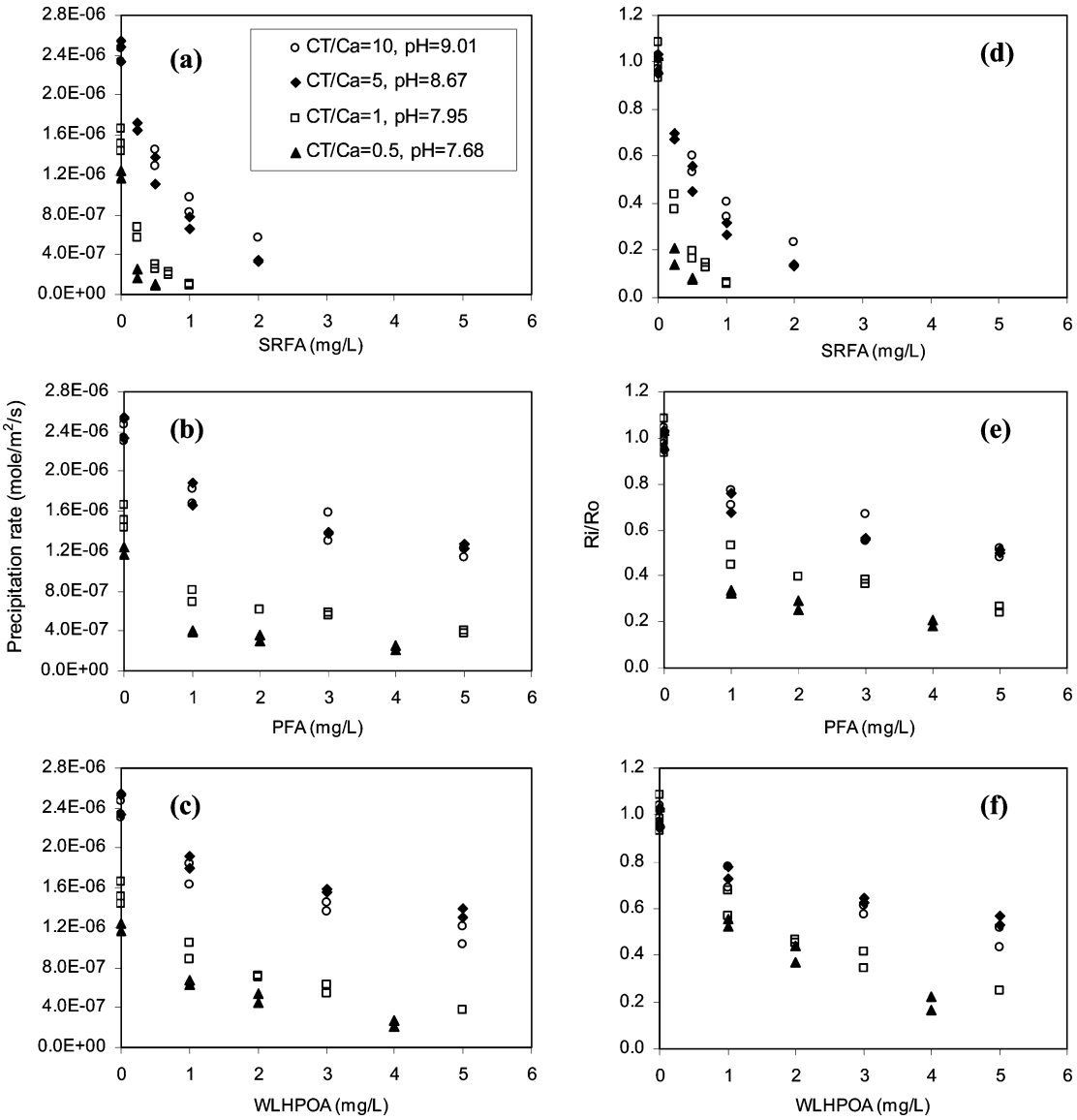

FIGURE 1. Inhibition of calcite precipitation as a function of NOM concentration ($\Omega = 5.3$, $I = 0.1$, 25 °C): (a) SRFA, (b) POFA, (c) WLHPOA. (d−f) Relative rate reduction.

al. (*13*) and Pokrovsky et al. (*14*). The surface complexation reactions and their intrinsic stability constants, K^0_{int}, are summarized in Table S3 in the Supporting Information. A surface density of 5 sites/nm^2 was assigned for both calcium and carbonate sites (*26*) for the calcite seed employed, and a constant capacitance model was used (*14*), with a double layer capacitance of $I^{1/2}/0.006$ (F/m^2), where I is the ionic strength. The surface charge of calcite, unlike oxide mineral surfaces, is not only a function of pH but is also dependent on solution composition (*27*−*29*). It should be noted that surface complexation reactions were treated in the same manner as solution-phase reactions. Thus, surface-reactive sites were presumed to be distributed homogeneously on the calcite surface with the same reactivity regardless of the morphology of the surface where they were located.

Results and Discussion

Kinetics and Mechanism of Calcite Precipitation in the Presence of NOM. The reductions in the calcite precipitation rate as a function of NOM concentration for the three different types of NOM and for four different solution compositions with the same degree of supersaturation ($\Omega = 5.3$) are presented in Figures 1a−c. The relative reductions in the precipitation rates, expressed as R_i/R_0 (R_0 is the precipitation rate in the absence of NOM, and R_i is the precipitation rate in the presence of NOM), as a function of NOM concentration are also shown in Figures 1 d−f. In the absence of NOM, the calcite precipitation rates (R_0) were different for the four different solution compositions, indicating that the degree of supersaturation is not the sole parameter affecting the kinetics of calcite precipitation (*30*−*34*). The differences in the precipitation rates result from the different densities of the active crystal growth sites on the calcite surface induced by the different species concentrations at the calcite−water interface under different solution compositions. From our previous work (*16*), we identified the active crystal growth sites on the calcite surface as $>CaCO_3^-$ and $>CO_3^-$. Details of the effects of solution composition on the concentrations of these two surface species and a kinetic model of heterogeneous calcite precipitation in the absence of inhibitor can also be found in the same work.

In general, SRFA exhibited the strongest inhibitory behavior, and PFA and WLHPOA showed similar inhibitory effects on calcite precipitation. The inhibition by the three NOMs was more pronounced at lower C_T/Ca^{2+} ratios or lower pH values as shown in Figure 1. To explain this solution-

composition-dependent inhibition, both calcite surface speciation and NOM speciation for the different solution compositions need to be considered. A detailed discussion of these considerations is presented below.

The adsorption of NOM onto various mineral surfaces has been suggested to follow Langmuir adsorption theory (*9*, *35*, *36*). We propose that the adsorption of NOM onto the calcite surface causes the observed inhibition and that the adsorption on this surface also follows Langmuir theory as described in eq 3

$$>S^- + NOM = >S^- - NOM \quad K_{cond} = \frac{[>S^- - NOM]}{[>S^-][NOM]} \quad (3)$$

where $>S^-$ represents the free active crystal growth sites on the calcite surface, $>S^- - NOM$ represents the sites at which NOM is adsorbed, and K_{cond} is a "conditional" equilibrium constant. The concentration of the free active crystal growth sites in the presence of NOM can be expressed as

$$[>S^-] = \frac{[>S^-]_T}{1 + K_{cond}[NOM]} \quad (4)$$

where $[>S^-]_T$ represents the density of the total active crystal growth sites.

Assuming that the precipitation rate is proportional to the concentration of available active sites on the calcite surface, the precipitation rate in the absence of NOM, R_0, and the precipitation rate in the presence of NOM, R_i, are proportional to $[>S^-]_T$ and $[>S^-]$, respectively

$$R_0 \propto [>S^-]_T \quad (5)$$

$$R_i \propto [>S^-] = \frac{[>S^-]_T}{1 + K_{cond}[NOM]} \quad (6)$$

The normalized change in the precipitation rate due the varying NOM concentrations is expressed by eq 7

$$\frac{R_0 - R_i}{R_i} = K_{cond}\,[NOM] \quad (7)$$

The normalized change in the precipitation rates as a function of NOM concentration is shown in Figures 2a−c, with the regression lines forced through the origin. The linear relationship for each experimental system supports the proposed Langmuir adsorption model, and the slope is defined as the conditional equilibrium constant.

The conditional equilibrium constant increases with decreasing C_T/Ca^{2+} ratios and/or pH values, corresponding to more effective calcite growth inhibition at lower C_T/Ca^{2+} ratios and/or lower pH values. A similar impact of pH on the adsorption of NOM onto mineral surfaces has also been observed for iron oxide (*35*, *37*−*39*), aluminum oxide (*36*), and kaolinite (*40*). The reason suggested for this effect in these previous studies is that the surface charge of these minerals shifts toward more negative values as pH is increased, resulting in a stronger electrostatic repulsion against the negatively charged NOM molecules. In our system, however, the inhibition of calcite precipitation at lower C_T/Ca^{2+} ratios and/or lower pH values might be more complex because (1) the surface charge of calcite is not a function of pH per se but is related to the excess surface-potential-determining ions, Ca^{2+} or CO_3^{2-} (*27*−*29*), and (2) excess Ca^{2+} was present in our working solutions, resulting in the formation of dissolved NOM−Ca^+ complexes that could change the affinity of the NOM molecules toward the calcite surface and/or reduce the degree of supersaturation.

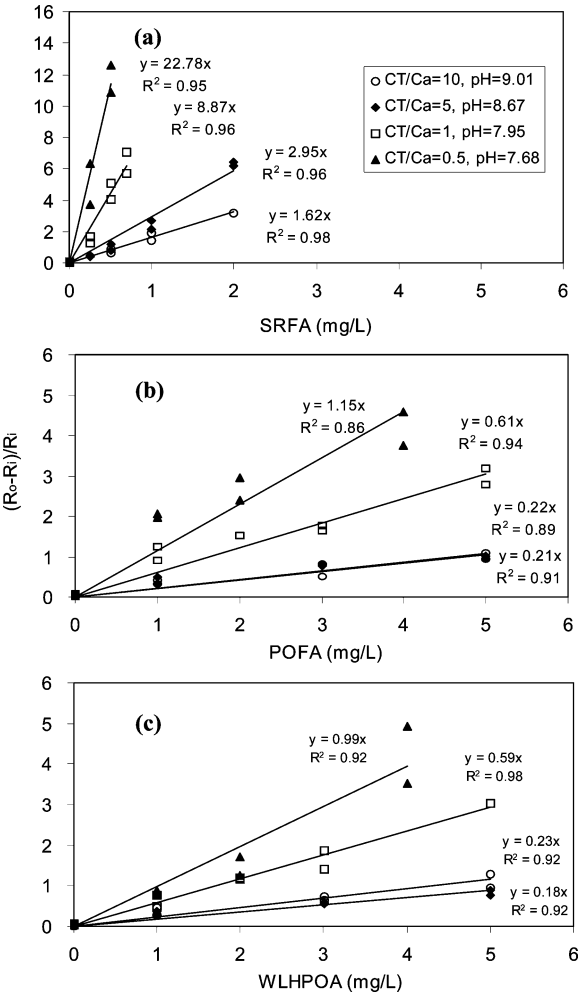

FIGURE 2. Normalized change in calcite precipitation rate as a function of NOM concentration (eq 7): (a) SRFA, (b) POFA, (c) WLHPOA. The slope is the value of the conditional equilibrium constant K_{cond}.

In an attempt to understand the reason for the variation in K_{cond} values with solution composition, we determined the charge density of the three NOMs as a function of pH and calculated the surface charge of the calcite based on surface complexation theory under our experimental conditions. The results are shown in Figure 3. The charge density of the NOMs showed only a small variation of about 0.4 mequiv/g over the experimental pH range 7.68−9.01, suggesting that deprotonation of carboxyl and/or phenolic groups does not vary significantly over this pH range. The surface of calcite, however, changes markedly from positively charged to negatively charged over this pH range.

NOM can form soluble complexes with Ca^{2+} through carboxylic acid moieties at neutral pH and through phenolic hydroxyl groups at alkaline pH (*41*). The formation of dissolved NOM−Ca complexes can have two effects on the precipitation rate of calcite to (1) reduce the free Ca^{2+} activity and the degree of supersaturation, thereby decreasing the rate of calcite precipitation, and (2) change the charge of the NOM molecules and thereby affect the adsorption of NOM onto active crystal growth sites on the calcite surface.

The first effect can be evaluated by assuming that a monodentate complex is formed between Ca^{2+} and a complexing site on the NOM molecule and that all deprotonated sites on the NOM molecule are complexed by Ca^{2+}. It should be noted that monodentate complex formation has been experimentally observed under low Ca^{2+} loading (*42*), has been successfully used for modeling calcium

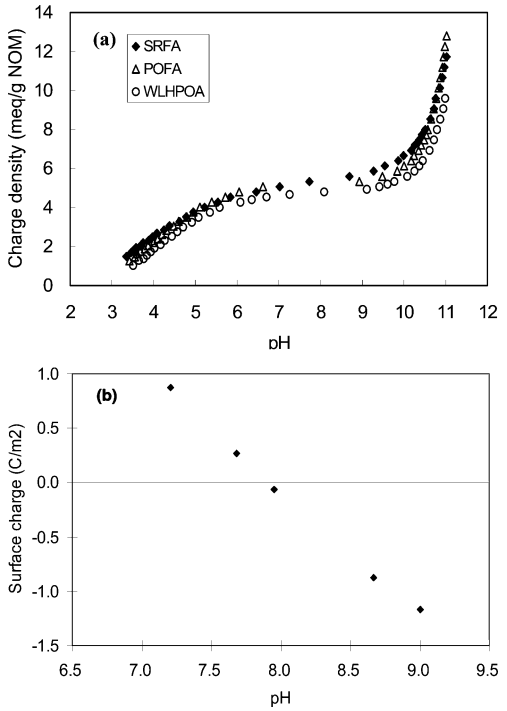

FIGURE 3. (a) Charge density of NOMs and (b) surface charge of calcite as a function of pH.

complexation of aquatic fulvic acid (*43*), and should be favored in our system because of the high ratio of Ca^{2+} to complexing sites employed in all solution compositions. Under our experimental conditions, the percent decrease in the free calcium concentration due to such assumed monodentate complexation can be calculated from the calcium concentration employed under each experimental condition (Table S1) and the NOM binding site concentration estimated from the charge density curve (Figure 3a) for each experimental pH value. The percent decrease ranges from 0.075% to 3% of the free calcium concentration in the absence of NOM, lowering the degree of supersaturation, Ω, by only 0.004−0.173. In comparison to the rate reduction observed and illustrated in Figure 1 ($R_i/R_0 = 6-70\%$), the loss of Ca^{2+} due to the formation of dissolved NOM−Ca complexes does not appear to be an important factor in inhibiting calcite precipitation. Instead, the change in the adsorption behavior of NOM on the calcite surface with changes in pH and total calcium concentration is the most likely mechanism responsible for the observed calcite precipitation rate reduction.

Careful examination of eq 7 indicates that the "conditional" feature of K_{cond} results from the failure to identify the species of NOM (NOM^-, $NOM-Ca^+$, or both) involved in the adsorption reaction (eq 3). The surface species responsible for calcite crystallization are $>CaCO_3^-$ and $>CO_3^-$, as shown in our previous work (*16*), and they should have similar reactivities because of their similar surface functional group nature. On the basis of electrostatic considerations, we believe that the primary species of NOM adsorbed on these negatively charged sites is $NOM-Ca^+$. The adsorption of NOM^- on these sites is discounted, although NOM^- may still occupy a small fraction of these sites through a ligand-exchange mechanism (*1*). The favorable adsorption of $NOM-Ca^+$ onto these negatively charged sites most likely contributes to the solution-composition-dependent inhibition shown in Figure 1. Due to the higher Ca^{2+} concentrations present at lower pH values and C_T/Ca^{2+} ratios (C_T is the same for all solution compositions), the formation of greater amounts of $NOM-Ca^+$ complexes is expected, which may result in more extensive adsorption of these complexes onto the negatively charged $>CaCO_3^-$ and $>CO_3^-$ sites even though the net charge of the calcite surface is more positive at lower pH values. Therefore, if we can determine the concentrations of $NOM-Ca^+$ in our working solutions, then the conditional K values shown in Figure 2 might converge to a single "nonconditional" equilibrium constant for the following reaction

$$>S^- + NOM-Ca^+ = >S-Ca-NOM \qquad K_{noncond} = \frac{[>S-Ca-NOM]}{[>S^-][NOM-Ca^+]} \quad (8)$$

Equation 7 can also be rewritten as follows

$$\frac{R_0 - R_i}{R_i} = K_{noncond}[NOM-Ca^+] \quad (9)$$

By comparison of eqs 7 and 9 for the observed normalized change in precipitation rates, the nonconditional equilibrium constant can be expressed in terms of the conditional equilibrium constant by the following equation

$$K_{noncond} = K_{cond}\frac{[NOM]}{[NOM-Ca^+]} \quad (10)$$

where [NOM] is the concentration of SRFA, POFA, or WLHPOA expressed in molar units and $[NOM-Ca^+]$ is the site concentration expressed as equivalents per liter.

To estimate the extent of NOM complexation with Ca^{2+}, a stability constant for the $NOM-Ca^+$ complex is needed. Values of this stability constant (log K) reported in the literature range from 1.43 to 3.12 for NOM from different sources (*42*−*45*). However, these stability constants, again, are conditional constants (they are dependent on pH, ionic strength, Ca^{2+} concentration, and ligand concentration) and were often determined at high NOM concentrations. Thus, they may not be directly applicable to our system. Accordingly, another approach was taken to resolve this issue. First, we assumed that the complexation of Ca^{2+} by NOM can be described by assuming that NOM has only one type of binding site for Ca^{2+} under the conditions of our study, and a corresponding stability constant, K_s, is assigned to the complexation reaction

$$NOM^- + Ca^{2+} = NOM-Ca^+ \qquad K_s = \frac{[NOM-Ca^+]}{[NOM^-][Ca^{2+}]} \quad (11)$$

where $[NOM^-]$ is the deprotonated site concentration of NOM. At each pH value, the initial $[NOM^-]$ was estimated from the product of the total concentration of NOM and the charge density at that pH (Figure 3a). Second, $[NOM-Ca^+]$, $K_{noncond}$, and K_s were calculated employing eqs 10 and 11 and using an iterative approach until the values of $K_{noncond}$ converged to a single value at all pH values. It should be noted that the ionic strength was maintained at 0.1 for all of our working solutions and the variation of K_s with pH is not significant in the pH range of 7−9 (*43*). A unique value of K_s was able to describe the complexation of NOM^- by Ca^{2+} in our system. The values of K_s and $K_{noncond}$ for the three NOMs determined by this iteration processes, at 25 °C, are shown in Table 1. The coefficients of variation (CVs) for the nonconditional stability constants for each of the NOMs were 18.0% for SRFA, 26.4% for POFA, and 17.5% for WLHPOA.

All $K_{noncond}$ values showed reasonable convergence, and SRFA was about 50 times stronger as an inhibitor of calcite precipitation than POFA and WLHPOA in terms of the relative ratios of the site-specific equilibrium constants. Surprisingly, the values of $K_{noncond}$ for POFA and WLHPOA showed no statistically significant differences. It should be noted that

TABLE 1. Determination of the Values of $K_{noncond}$ (L/equiv) for SRFA, POFA, and WLHPOA at 25 °C[a]

pH	K_{cond} (L/mg)	K_{cond} (M^{-1})	SRFA ($K_s = 50$) charge density (mequiv/g FA)	[NOM]/[NOM−Ca^+]	$K_{noncond}$ (L/equiv)
7.68	22.78	3.10×10^7	5.3	0.49	1.50×10^7
7.95	8.87	1.21×10^7	5.45	0.81	9.77×10^6
8.67	2.95	4.01×10^6	5.6	3.42	1.37×10^7
9.01	1.62	2.20×10^6	5.7	6.58	1.45×10^7
				average	1.33×10^7
				standard deviation	0.24×10^7
				CV (%)	18.0

pH	K_{cond} (L/mg)	K_{cond} (M^{-1})	POFA ($K_s = 350$) charge density (mequiv/g FA)	[NOM]/[NOM−Ca^+]	$K_{noncond}$ (L/equiv)
7.68	1.15	6.12×10^5	5.19	0.49	2.99×10^5
7.95	0.61	3.25×10^5	5.22	0.62	2.00×10^5
8.67	0.22	1.17×10^5	5.30	1.62	1.88×10^5
9.01	0.21	1.12×10^5	5.37	2.86	3.16×10^5
				average	2.51×10^5
				standard deviation	0.66×10^5
				CV (%)	26.4

pH	K_{cond} (L/mg)	K_{cond} (M^{-1})	WLHPOA ($K_s = 350$) charge density (mequiv/g FA)	[NOM]/[NOM−Ca^+]	$K_{noncond}$ (L/equiv)
7.68	0.99	7.64×10^5	4.73	0.37	2.84×10^5
7.95	0.59	4.55×10^5	4.78	0.46	2.10×10^5
8.67	0.23	1.78×10^5	4.88	1.22	2.16×10^5
9.01	0.18	1.39×10^5	4.92	2.15	2.93×10^5
				average	2.51×10^5
				standard deviation	0.44×10^5
				CV (%)	17.5

[a] The values of K_s resulting in the best convergence of $K_{noncond}$ (smallest CV) for each NOM are also shown.

the K_s values determined by this iterative calculation are consistent with those reported in the literature (*42*−*45*).

The convergence of $K_{noncond}$ for these three NOMs with distinctly different physical/chemical characteristics indicates that the complexation of NOM with Ca^{2+} in the solution phase facilitates the adsorption process as a result of reducing electrostatic repulsion forces as described earlier. The enhanced adsorption of NOM onto mineral surfaces in the presence of Ca^{2+} has been reported for iron oxide (*37*) and aluminum oxide (*36*). A study by Tipping (*37*) found that the adsorption capacity for humic substances on iron oxides was doubled in a medium containing the divalent cations Ca^{2+} and Mg^{2+} compared to that in a medium containing the monovalent cation Na^+ at a pH value below the isoelectric point of the oxide, where the oxide surface is positively charged. It was postulated in that study that the enhanced adsorption resulted from competition between the divalent cations and the positively charged surface sites for the anionic groups associated with the humic substances, leading to fewer contacts per molecule with the oxide surface and allowing more humic substances to adsorb. This mechanism, however, may not be relevant to our system because the net charge of calcite was negative for most of our experimental conditions. Schlautman and Morgan (*36*) reported that the presence of 1 mM Ca^{2+} increased the adsorption of NOM onto aluminum oxide relative to a NaCl solution with the same ionic strength at almost all pH values. They attributed this effect to the formation of an outer-sphere surface complex through a "water bridging" mechanism in which Ca^{2+} ions were adsorbed on the surface first followed by the adsorption of anionic NOM on the Ca-regulated surface sites, with no displacement of water from the solvation shell of the Ca^{2+} ion. However, water bridging is an unlikely mechanism to explain the enhanced adsorption of NOM onto calcite in the presence of Ca^{2+} because (1) the complex of Ca^{2+} and NOM can be an inner-sphere complex (no water molecule between $Ca^{2+}$and binding sites on the NOM molecule) (*41*) and (2) Ca^{2+} is one of the lattice ions of calcite and dehydration might be possible when the NOM−Ca^+ complex ion is adsorbed on the calcite surface, i.e., no water molecule between NOM−Ca^+ and the calcite surface. The enthalpy change data for the adsorption reaction presented in the following section supports this hypothesis.

Thermodynamics of Adsorption of NOM onto the Calcite Surface. The well-characterized nature of the three NOMs examined in this study (see above and Table S2) allows for a determination of the thermodynamics of the adsorption reaction. By application of the weight-average molecular weight (M_w) of the three NOMs, the free energy ($\Delta G^{\circ\prime}$) of the adsorption reaction (eq 8) for each of the NOMs at 25 °C can be estimated

$$\Delta G^{\circ\prime} = -RT \ln K_{noncond} \quad (12)$$

where R is the ideal gas constant and T is the absolute temperature. (The reason we use $\Delta G^{\circ\prime}$ is that $K_{noncond}$ is derived from concentrations rather than activities.)

To understand the nature of the interaction between the NOM molecules and the calcite surface, we need to know the enthalpy change ($\Delta H^{\circ\prime}$) and entropy change ($\Delta S^{\circ\prime}$) of the adsorption reaction. At equilibrium, the free energy is related to the enthalpy change and entropy change through the following equation

$$\Delta G^{\circ\prime} = \Delta H^{\circ\prime} - T\Delta S^{\circ\prime} \quad (13)$$

Substituting eq 12 into eq 13 gives the following relationship

$$\ln K_{\text{noncond}} = -\frac{\Delta H^{\circ\prime}}{RT} + \frac{\Delta S^{\circ\prime}}{R} \quad (14)$$

Equation 14 is the integrated form of the van't Hoff equation, with the assumptions that $\Delta H^{\circ\prime}$ and $\Delta S^{\circ\prime}$ are independent of temperature (*46*). The value of $\Delta H^{\circ\prime}$ and $\Delta S^{\circ\prime}$ for the adsorption reaction can be determined from the slope and *y*-intercept of a plot of ln K_{noncond} versus T^{-1}.

The K_{cond} values (slopes) at different temperatures for each of the NOMs, analogous to the results in Figure 2, and the K_{noncond} values calculated from K_{cond} using the K_s values determined at 25 °C are shown in Figure S3 and Table S4, respectively, in the Supporting Information. The plots of ln K_{noncond} versus T^{-1} according to eq 14 are shown in Figure 4 for all three NOMs. Thermodynamic data for each of the NOMs at 25 °C are presented in Table 2. The highest adsorption energy ($\Delta G^{\circ\prime}$) was observed for SRFA, and those for WLHPOA and POFA were identical because they had the same K_{noncond} at 25 °C. It should be noted that, at other temperatures, the inhibitory behavior of WLHPOA and POFA were different (Figure 4). Adsorption of the three NOMs onto the calcite surface are all endothermic reactions (positive $\Delta H^{\circ\prime}$), with the highest $\Delta H^{\circ\prime}$ for WLHPOA, followed by SRFA and POFA. In addition, all adsorption reactions were driven by entropy change, most likely resulting from the release of water molecules from the calcite surface to compensate for the adsorption of the NOM molecules. The high values of $\Delta H^{\circ\prime}$ also suggest that the adsorption of these NOMs onto the calcite surface is a chemisorption or specific adsorption reaction, i.e., no water molecule exists between the bound NOM−Ca^+ and the calcite surface. Thus, the reaction responsible for the reduction in the rate of calcite precipitation can be further revised from eq 8 to the following

$$>S^- - nH_2O + NOM - Ca^+ = >S - Ca - NOM + nH_2O$$

$$K_{\text{noncond}} = \frac{[>S - Ca - NOM]}{[>S^- - H_2O][NOM - Ca^+]} \quad (15)$$

The endothermic adsorption of humic materials has also been reported for kaolinite (*47*−*48*). Ghabbour et al. (*47*) studied the sorption of humic acids derived from different sources onto kaolinite and found that the adsorption reactions were primarily endothermic. They also suggested that the dehydration of kaolinite and humic acid were responsible for the entropy increases during adsorption. Zhou et al. (*48*) investigated adsorption of four different humic substances onto kaolinite under simulated estuarine conditions and reported that two of the four humic substances exhibited endothermic adsorption. They proposed that the endothermic property resulted from the chemisorption of these humic substances, which required a substantial activation energy.

Characteristics of NOM and Inhibition of Calcite Precipitation. NOM with higher molecular weight has been reported to be a stronger inhibitor of calcium carbonate precipitation due to its greater polymeric character and associated stereochemical effects (*5*, *7*). In this study, SRFA, the NOM with the highest molecular weight, showed the strongest inhibitory effect on calcite precipitation. There was no statistically significant difference in the inhibition exhibited by POFA and WLHPOA at 25 °C, although they possess different molecular weights. The similar K_{noncond} (or $\Delta G^{\circ\prime}$) for POFA and WLHPOA, however, derives from different thermodynamic properties of the adsorption reaction, which compensate for each other. As shown in Table 2, the strength of the bond ($\Delta H^{\circ\prime}$) between WLHPOA and the crystal growth sites on the calcite surface is about twice that for POFA, and in turn, a higher entropy change ($T\Delta S^{\circ\prime}$) must result from the adsorption of WLHPOA than that from POFA to make them indistinguishable in their net inhibitory effect on calcite precipitation (same $\Delta G^{\circ\prime}$). Thus, molecular weight may not be the sole factor determining the inhibition of calcite precipitation, especially when comparing NOMs with similar molecular size.

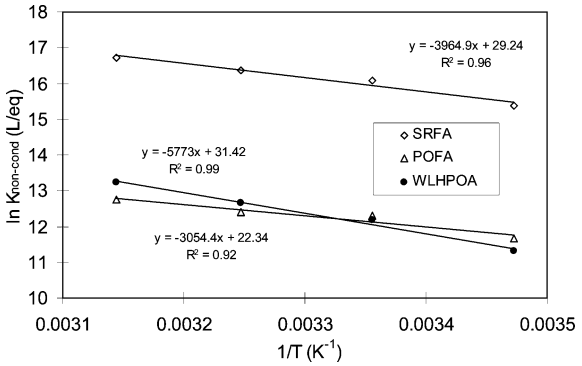

FIGURE 4. van't Hoff plot of nonconditional stability constants at different temperatures. The slope is equal to $-\Delta H^{\circ\prime}/R$.

TABLE 2. Summary of Thermodynamic Data for the Chemisorption of NOM onto Calcite (25 °C)

	SRFA	POFA	WLHPOA
$\Delta G^{\circ\prime}$ (kJ/equiv)	−40.6	−30.8	−30.8
$\Delta H^{\circ\prime}$ (kJ/equiv)	33.0	25.4	48.0
$T\Delta S^{\circ\prime}$ (kJ/equiv)	72.8	56.5	77.9

It is generally accepted that the aromatic content of NOM correlates directly to its molecular weight (*24*) and contributes most to the ability of NOM to inhibit calcite precipitation (*3*−*5*). Thus, the strongest degree of inhibition observed for SRFA should be a combined result of its high molecular weight and high aromatic carbon content, although SRFA also had the highest hydrophilic (aliphatic II, carboxyl, and ketone) content.

The molecular weight and aromatic carbon content of POFA and WLHPOA were different, but similar inhibitory effects were observed. This similarity results from a counterbalancing of the different thermodynamic properties of the adsorption reaction; both enthalpy change and entropy change were higher for WLHPOA than those for the POFA as shown in Table 2. WLHPOA has a greater aromatic carbon content and has less hydrophilic moieties than POFA (Table S2). It is not surprising that the stronger hydrophobic nature of WLHPOA would cause a higher entropy change during its adsorption on calcite because more water molecules would need to be displaced from the calcite surface due to this hydrophobic effect (*1*). However, it is surprising that the differences between the enthalpy change and the entropy change ($\Delta H^{\circ\prime} - T\Delta S^{\circ\prime}$) for WLHPOA and POFA were the same at 25 °C.

In summary, the inhibition of calcite precipitation by NOM can be described by the Langmuir adsorption theory, i.e., that the rate of calcite precipitation is proportional to the available active crystal growth sites on the calcite surface. Traditionally, data-fitting to the Langmuir adsorption isotherm usually results in a conditional equilibrium constant or an adsorption constant that is highly dependent on pH because of difficulties in identifying the actual sites on the adsorbent and adsorbate that participate in the adsorption reaction. In this study, we were able to converge disaggregated conditional equilibrium constants determined at different solution compositions to a single nonconditional value by assuming that the sites on the NOM macromolecule complexed by Ca^{2+} (NOM−Ca^+) are the responsible sites that adsorb to crystal growth sites on the calcite surface and

subsequently inhibit calcite precipitation. This mechanism can be used to explain the degree of supersaturation with respect to calcite that is normally observed in natural waters rich in NOM (*3*). In addition, this degree of supersaturation may be higher if the molecular weight and hydrophobic content of the NOM are greater. The high positive enthalpy change of the adsorption reaction suggests that the adsorption of NOM onto the calcite surface is a chemisorption process and that the reaction is endothermic. In addition, the adsorption reaction is driven solely by the entropy change, most likely resulting from the release of water molecules on the calcite surface that accompanies the adsorption of the hydrophobic NOM macromolecules. The greatest inhibitory effect was observed for the NOM with the highest molecular weight and aromatic content. However, molecular weight and aromatic content may not be the only determining factors. The balance between enthalpy change and entropy change should determine the extent to which NOM inhibits the rate of calcite precipitation.

Acknowledgments

The authors thank Procter and Gamble for supporting this research. The authors also thank Dr. Russell Christman and Dr. Larry Benninger of the University of North Carolina for valuable discussion and comment reflected in this paper.

Supporting Information Available

Additional text and tables. This material is available free of charge via the Internet at http://pubs.acs.org.

Literature Cited

(1) Stumm, W.; Morgan, J. J. *Aquatic Chemistry*, 3rd ed.; Wiley-Interscience: New York, 1996.
(2) Chave, K.; Seuss, E. Calcium carbonate supersaturation in seawater: Effects of dissolved organic matter. *Limnol. Oceanogr.* **1970**, *15*, 633−637.
(3) Reynolds, R. C. Polyphenol inhibition of calcite precipitation in Lake Powell. *Limnol. Oceanogr.* **1978**, *23*, 585−597.
(4) Inskeep, W. P.; Bloom, P. R. Kinetics of calcite precipitation in the presence of water soluble organic ligands. *Soil Sci. Soc. Am. J.* **1986**, *50*, 1167−1172.
(5) Hoch, A. R.; Reddy, M. M.; Aiken, G. R. Calcite crystal growth inhibition by humic substances with emphasis on hydrophobic acids from the Florida Everglades. *Geochim. Cosmochim. Acta* **2000**, *64*, 61−72.
(6) Furrer, G.; Stumm, W. The coordination chemistry of weathering. 1. Dissolution kinetics of δ-Al_2O_3 and BeO. *Geochim. Cosmochim. Acta* **1986**, *50*, 1847−1860.
(7) Berner, R. A.; Westrich, J. T.; Graber, R.; Smith, J.; Martens, C. S. Inhibition of aragonite precipitation from supersaturated seawater: A laboratory and field study. *Am. J. Sci.* **1978**, *278*, 816−837.
(8) Lebron, I.; Suarez, D. L. Calcite nucleation and precipitation kinetics as affected by dissolved organic matter at 25 °C and pH > 7.5. *Geochim. Cosmochim. Acta* **1996**, *60*, 2765−2776.
(9) Lebron, I.; Suarez, D. L. Kinetics and mechanisms of precipitation of calcite as affected by P_{CO_2} and organic ligands at 25 °C. *Geochim. Cosmochim. Acta* **1998**, *62*, 405−416.
(10) Zuddas, P.; Pachana, K.; Faivre, D. The influence of dissolved humic acids on the kinetics of calcite precipitation from seawater solutions. *Chem. Geol.* **2003**, *201*, 91−101.
(11) Zullig, J. J.; Morse, J. W. Interaction of organic acids with carbonate mineral surfaces in seawater and related solutions. 1. Fatty acid adsorption. *Geochim. Cosmochim. Acta* **1988**, *52*, 1667−1678.
(12) Grossl, P. R.; Inskeep, W. P. Kinetics of octacalcium phosphate crystal growth in the presence of organic acids. *Geochim. Cosmochim. Acta* **1992**, *56*, 1955−1961.
(13) van Cappellen, P.; Charlet, L.; Stumm, W.; Wersin, P. A surface complexation model of the carbonate mineral−aqueous solution interface. *Geochim. Cosmochim. Acta* **1993**, *57*, 3505−3518.
(14) Pokrovsky, O. S.; Mielczarski, J. A.; Barres, O.; Schott, J. Surface speciation models of calcite and dolomite/aqueous solution interfaces and their spectroscopic evaluation. *Langmuir* **2000**, *16*, 2677−2688.
(15) Nilsson, O.; Sternbeck, J. A mechanistic model for calcite crystal growth using surface speciation. *Geochim. Cosmochim. Acta* **1999**, *63*, 217−225.
(16) Lin, Y. P.; Singer, P. C. Effects of seed material and solution composition on calcite precipitation. *Geochim. Cosmochim. Acta*, in press.
(17) Reddy, M. M.; Hoch, A. R. Calcite crystal growth rate inhibition by polycarboxylic acids. *J. Colloid Interface Sci.* **2001**, *235*, 365−370.
(18) Brunauer, S.; Emmet, P. H.; Teller, E. Adsorption of gases in multimolecular layers. *J. Am. Chem. Soc.* **1938**, *60*, 309−319.
(19) Aiken, G. R.; McKnight, D. M.; Thorn, K. A.; Thurman, E. M. Isolation of hydrophilic organic acids from water using nonionic macroporous resins. *Org. Geochem.* **1992**, *18*, 567−573.
(20) Aiken, G. R.; McKnight, D. M.; Harnish, R.; Wershaw, R. Geochemistry of aquatic humic substances in the Lake Fryxell Basin, Antarctica. *Biogeochemistry* **1996**, *34*, 157−188.
(21) Wilson, M. A. Applications of nuclear magnetic resonance spectroscopy to the study of the structure of soil organic matter. *J. Soil Sci.* **1981**, *32*, 167−186.
(22) Wershaw, R. In *Humic Substances in Soil, Sediment and Water: Geochemistry, Isolation, and Characterization*; Aiken, G. R., McKnight, D. M., Wershaw, R., MacCarthy, P., Eds.; John Wiley and Sons: New York, 1985; pp 561−582.
(23) Huffman, W. D.; Stuber, H. A. In *Humic Substances in Soil, Sediment and Water: Geochemistry, Isolation, and Characterization*; Aiken, G. R., McKnight, D. M., Wershaw, R., MacCarthy, P., Eds.; John Wiley and Sons: New York, 1985; pp 433−456.
(24) Chin, Y. P.; Aiken, G. R.; O'Loughlin, E. Molecular weight, polydispersity, and spectroscopic properties of aquatic humic substances. *Environ. Sci. Technol.* **1994**, *28*, 1853−1858.
(25) Gustafsson, J. P. *Visual MINTEQ*, version 2.30; Department of Land and Water Resources Engineering, The Royal Institute of Technology: Stockholm, Sweden, 2004; http://www.lwr.kth.se/english/OurSoftWare/Vminteq/.
(26) Davis, J. A.; Kent, D. B. In *Mineral−Water Interface Geochemistry*; Hochella, M. F., White, A. F., Eds.; Mineralogical Society of America: Washington, DC, 1990; pp 177−260.
(27) Thompson, D. W.; Pownall, P. G. Surface electrical properties of calcite. *J. Colloid Interface Sci.* **1989**, *131*, 74−82.
(28) Cicerone, D. S.; Regazzoni, A. E.; Blesa, M. A. Electrokinetic properties of the calcite water interface in the presence of magnesium and organic matter. *J. Colloid Interface Sci.* **1992**, *154*, 423−433.
(29) Stipp, S. L. S. Toward a conceptual model of the calcite surface: Hydration, hydrolysis, and surface potential. *Geochim. Cosmochim. Acta* **1999**, *63*, 3121−3131.
(30) Reddy, M. M.; Plummer, L. N.; Busenberg, E. Crystal growth of calcite from calcium bicarbonate solutions at constant P_{CO_2} and 25 °C: A test of a calcite dissolution model. *Geochim. Cosmochim. Acta* **1981**, *45*, 1281−1289.
(31) Morse, J. W. In *Carbonates: Mineralogy and Chemistry*; Reeder, R. J., Ed.; Reviews in Mineralogy 11; Mineralogical Society of America: Washington, DC, 1983; pp 227−264.
(32) Inskeep, W. P.; Bloom, P. R. An evaluation of rate equations for calcite precipitation kinetics at P_{CO_2} less than 0.01 atm and pH > 8. *Geochim. Cosmochim. Acta* **1985**, *49*, 2165−2180.
(33) Mucci, A. Growth kinetics and composition of magnesian calcite overgrowths precipitated from seawater—Quantitative influence of ortho-phosphate ions. *Geochim. Cosmochim. Acta* **1986**, *50*, 2255−2265.
(34) Shiraki, R.; Brantley, S. L. Kinetics of near equilibrium calcite precipitation at 100 °C: An evaluation of elementary reaction-based and affinity-based rate laws. *Geochim. Cosmochim. Acta* **1995**, *59*, 1457−1471.
(35) Wang, L. L.; Chin, Y. P.; Traina, S. J. Adsorption of (poly)maleic acid and an aquatic fulvic acid by goethite. *Geochim. Cosmochim. Acta* **1997**, *61*, 5313−5324.
(36) Schlautman, M. A.; Morgan, J. J. Adsorption of aquatic humic substances on colloidal-size aluminum oxide particles: Influence of solution chemistry. *Geochim. Cosmochim. Acta* **1994**, *58*, 4293−4303.
(37) Tipping, E. The adsorption of aquatic humic substances by iron oxides. *Geochim. Cosmochim. Acta* **1981**, *45*, 191−199.
(38) Gu, B. H.; Schmitt, J.; Chen, Z. H.; Liang, L. Y.; McCarthy, J. F. Adsorption and desorption of natural organic matter on iron oxide—Mechanisms and models. *Environ. Sci. Technol.* **1994**, *28*, 38−46.
(39) Saito, T.; Koopal, L. K.; van Riemsdijk, W. H.; Nagasaki, S.; Tanaka, S. Adsorption of humic acid on goethite: Isotherms, charge adjustments, and potential profiles. *Langmuir* **2004**, *20*, 689−700.

(40) Namjesnik-Dejanovic, K.; Maurice, P. A.; Aiken, G. R.; Cabaniss, S.; Chin, Y. P.; Pullin, M. J. Adsorption and fractionation of a muck fulvic acid on kaolinite and goethite at pH 3.7, 6, and 8. *Soil Sci.* **2000**, *165*, 545−559.

(41) Leenheer, J. A.; Brown, G. K.; MacCarthy, P.; Cabaniss, S. E. Models of metal binding structures in fulvic acid from the Suwannee River, Georgia. *Environ. Sci. Technol.* **1998**, *32*, 2410−2416.

(42) Brown, G. K.; MacCarthy, P.; Leenheer, J. A. Simultaneous determination of Ca, Cu, Ni, Zn and Cd binding strengths with fulvic acid fractions by Schubert's method. *Anal. Chim. Acta* **1999**, *402*, 169−181.

(43) Bose, P.; Reckhow, D. A. Modeling pH and ionic strength effects on proton and calcium complexation of fulvic acid: A tool for drinking water-NOM studies. *Environ. Sci. Technol.* **1997**, *31*, 765−770.

(44) Sposito, G. Trace metals in contaminated waters. *Environ. Sci. Technol.* **1980**, *15*, 396−403.

(45) Dempsey, B. A.; O'Melia, C. R. In *Aquatic and Terrestrial Humic Materials*; Christman, R. F., Gjessing, E. T., Eds.; Ann Arbor Science: Ann Arbor, MI, 1983.

(46) Schwarzenbach, R. P.; Gschwend, P. M.; Imboden, D. M. *Environmental Organic Chemistry*, 2nd ed.; Wiley: Hoboken, NJ, 2002.

(47) Ghabbour, E. A.; Davies, G.; Goodwillie, M. E.; O'Donaughy, K.; Smith, T. L. Thermodynamics of peat-, plant-, and soil-derived humic acid sorption on kaolinite. *Environ. Sci. Technol.* **2004**, *38*, 3338−3342.

(48) Zhou, J. L.; Rowland, S.; Mantoura, R. F. C.; Braven, J. The formation of humic coatings on mineral particles under simulated estuarine conditions—A mechanistic study. *Water Res.* **1994**, *28*, 571−579.

Received for review March 9, 2005. Revised manuscript received July 19, 2005. Accepted July 20, 2005.

ES050470Z